STANDOFF TRACE ANALYTE DETECTION USING

AMPLIFYING FLUORESCENT POLYMERS

By

ROBERT J. SLEEZER

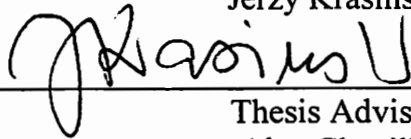Bachelor of Science
Oklahoma State University
Stillwater, Oklahoma
2004

Bachelor of Science
Oklahoma State University
Stillwater, Oklahoma
2004

Submitted to the Faculty of the
Graduate College of the
Oklahoma State University
in partial fulfillment of
the requirements for
the Degree of
MASTER OF SCIENCE
May, 2006

STANDOFF TRACE ANALYTE DETECTION USING

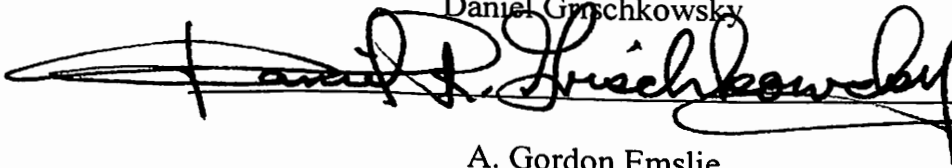# AMPLIFYING FLUORESCENT POLYMERS

Thesis Approved:

Jerzy Krasinski

Thesis Advisor

Alan Cheville

Daniel Grischkowsky

A. Gordon Emslie

Dean of the Graduate College

ACKNOWLEDGMENTS

TABLE OF CONTENTS

I.

LIST OF TABLES

LIST OF FIGURES

LIST OF SYMBOLS

A	Luminescent Compound
A/D	Analog to Digital Converter
AFP	Amplifying Fluorescent Polymer
CCD	Charge Coupled Device
CP	Conjugate Polymer
CTE	Charge Transfer Efficiency
I5	Average Intensity of a 5x5 Pixel Area Surrounding a Local Maxima
IAFP	Intensity of the Amplifying Fluorescent Polymer
Ib	Background Intensity
Ip	Local Maxima Intensity
φ_0	Quantum Efficiency of Donor in Absence of Quencher
φ_Q	Quantum Efficiency of Donor in Presence of Quencher
K_D	Dynamic Stern-Volmer Quenching Constant
K_s	Static Stern-Volmer Quenching Constant
K_{sv}	General Stern-Volmer Constant (either static or dynamic)
M	Monomer
MPS-PPV	Poly(2-methoxy-5-propfloxy sulfonate phenylene vinylene)

ν	Monomer Emission Frequency
n	Number of Electrons After a Process
ν_0	Excitation Frequency
n_0	Number of Electrons Before a Process
ν_1	Luminescent Compound Emission Frequency
Q	Quencher
r	Number of Rows
SBIG	Santa Barbra Instrument Group
SLO	Stem-Loop Oligonucleotide

1. INTRODUCTION

Standoff detection, or the process of discerning important information about a remote environment, is a critical issue for a diverse set of problems including explosives detection [1] and chemical and biological agent detection [2]. An experimental system was developed for detecting small amounts of chemicals containing fluorescence quenching groups in their structures, using standard off the shelf components, with minor modifications. An amplifying fluorescent polymer (AFP) was used as detector. The goal of this research was to demonstrate the ability of the AFP to detect the chemicals from a range of up to 60 meters.

This document will begin with a review of the literature that discusses the background of the AFP, including information about general conjugate polymers (CP), before moving on to a discussion of the imaging system. This will be followed by a discussion of other current standoff detection systems, their uses, and their operation. Next, a detailed definition of the problem solved by the developed system will be provided. A detailed presentation of the system, the experimental results, and considerations for improving the system is included.

2. REVIEW OF THE LITERATURE

The two technologies that were studied as a part of this research, AFPs and low noise

high sensitivity CCDs, are discussed in this section. The AFP used in the experiments

was provided for us by an external source; however, because it is such an integral part of

the system, it is important to understand the mechanics and the choices available. The

specific AFP used in this case is proprietary and discussion of it, as well as the chemical

analyte, is limited by possible Export Administration Regulations or International Arms

Trade Regulations. The AFP used in this research was designed to be both highly

selective and efficiently quenched by the chosen analyte. The choice of the CCD allowed

for significantly more flexibility. The information presented in this section highlights the

reasons the CCD was chosen for this research and provides a basis for making further

decisions about creating a practical real-time system for detecting the analyte.

2.1 Amplifying Fluorescent Polymers

Many types of Conjugate Polymer (CP) based sensors have been developed for specific

applications. These types include conductometric sensors that show a change in

conductance, potentiometric sensors that show a change in chemical potential,

colorimetric sensors that show a change in absorption [3].

The CP sensor used in this research falls into a different category than those previously mentioned. It relies on the fluorescence properties to change in the presence of a specific chemical analyte. Specifically, the fluorescence efficiency decreases as the concentration of the analyte increases. The rest of this section is dedicated to presenting the theory behind the quenching and to discussing of other polymers that operate on the same principle.

2.1.1 The Process of Fluorescence Quenching

The concept of using fluorescence quenching as a sensor was developed by George Stokes who saw applications in the area of detecting organic substances [4]. The process of fluorescence is outlined very well by Barashkov and Gunder in [5] where they discuss processes for a polymer consisting of some monomer M, quencher Q, luminescent compound A, at an excitation frequency v_0, emission frequency of monomer v, and emission frequency of luminescent compound v_1. The equations below show these processes.

$$M_0 + h v_0 \xrightarrow{k_0} M^* \tag{1}$$

$$M^* \xrightarrow{k_d} M_0 \tag{2}$$

$$M^* \xrightarrow{k1} M_0 + h v \tag{3}$$

$$M_0 + M^* \xrightarrow{k_r} (M_0 M^*) \tag{4}$$

$$M^{\bullet} + Q_0 \xrightarrow{k_q} Q^{\bullet} + M_0 \tag{5}$$

$$Q^{\bullet} \rightarrow Q_0 \tag{6}$$

$$M^{\bullet} + A_0 \rightarrow A^{\bullet} + M_0 \tag{7}$$

$$(M_0 M^{\bullet}) + A_0 \rightarrow A^{\bullet} + 2M_0 \tag{8}$$

$$Q^{\bullet} + A_0 \rightarrow A^{\bullet} + Q_0 \tag{9}$$

$$A^{\bullet} \rightarrow A_0 + h\nu_1 \tag{10}$$

$$A^{\bullet} \rightarrow A_0 \tag{11}$$

M_0 is excited to $M^{\bullet}$ at a rate defined by k_0. Likewise, $M^{\bullet}$ decays to M_0 nonradiatively (no photon emission) and radiatively at rates defined by k_d and k_l respectively. In a similar manner, k_e defines the rates for eximer (excited dimmer) formation from M_0 and $M^{\bullet}$ while k_q defines the rate that an excited monomer will transfer its energy to quenching atom in the ground state. In the case of this research, there is no luminescent compound so equations (7) through (11) do not apply. From this point, [5] goes on to develop the Stern-Volmer equation for the dynamic or collisional case

$$\frac{\varphi_0}{\varphi_Q} = 1 + \frac{k_q}{k_l + k_d}[Q] \tag{12}$$

where φ_0 and φ_Q is the quantum efficiency of the donor molecule in the absence and the presence of quencher respectively and $[Q]$ is the concentration of the quencher. The group of constants in front of $[Q]$ are often referred to as the dynamic Stern-Volmer

constant K_D. Equation 17 works well for low $[Q]$, however, as $[Q]$ increases, it becomes

increasingly difficult for each analyte molecule to be in the area of a donor that does not

have an analyte already nearby. Additionally, the efficiency of the energy transfer from

the donor to the quencher is not considered. So, (12) is developed further to

$$\frac{\varphi_0}{\varphi_Q} = \frac{1 + \dfrac{k_q}{k_1 + k_d}[Q]}{1 + \alpha u} \tag{13}$$

Where α equals the efficiency of the energy transfer and u is the fraction of donors that

have a quencher nearby [5].

A second approach was taken by [6] where both static and dynamic quenching are

considered. The equation developed is

$$\frac{\varphi_0}{\varphi_Q} = \left(1 + \frac{k_q}{k_1 + k_d}[Q]\right)(1 + K_S[Q]) \tag{14}$$

where K_S, often referred to as the static Stern-Volmer constant, is the association

constant, for complex formation and is given by

$$K_S = \frac{[F - Q]}{[F][Q]} \tag{15}$$

where [F-Q] and [F] are the concentrations of the complex and the fluorophore respectively. So, it is possible to discern the amount of quencher present in the system if k_q, k_1, k_d, and φ_0 are known and φ_Q is measured. In the case of the AFP used for this research, the analyte binds to the polymer meaning the quenching is dominated by the static process. As a result, (14) is reduced to

$$\frac{\varphi_0}{\varphi_Q} = \left(1 + K_s[Q]\right) \tag{16}$$

and the results of a plot of this equation would be expected to be linear with slope K_s [7]. If the process were dominated by dynamic quenching, (14) is reduced to

$$\frac{\varphi_0}{\varphi_Q} = \left(1 + K_D[Q]\right) \tag{17}$$

which is expected to be linear with slope K_D. The experiments conducted for this work are intended to demonstrate the overall functionality of the system rather than provide a fine-tuning mechanism. However, equations (14), (16), and (17) demonstrate that a practical method based on fluorescence intensity measurement can be developed not only for positive identification of the analyte but also for analyte concentration.

2.1.2 Fluorescence Quenching Amplification

Amplification of the fluorescence quenching ability of the analyte is critical to detecting trace quantities of the analyte [8]. In essence, the fluorescence quenching amplification is done by connecting a series of chromophores such that one molecule of analyte is sufficient to quench the entire chain. The result of this configuration is essentially an increase of the constants K_s in (16) and K_D in (17) [7]. The next paragraph presents a brief discussion of the mechanics of AFPs.

In the creation of an AFP, the chromophores are connected in series by a conjugate polymer. This is referred to as the molecular wire approach because it allows for energy migration along the polymer, which results in quenching if the lifetime is sufficiently long and there is at least one quencher is present [7]. A conceptualization of this approach is shown in Figure 1 where PQ^{+2} acts as the quencher [7]. The end result of using a molecular wire is to dramatically increase the Stern-Volmer constant significantly. Again, assuming a sufficient life time and rapid energy migration, the Stern-Volmer constant would be increased by the number of chromophores in the polymer [7].
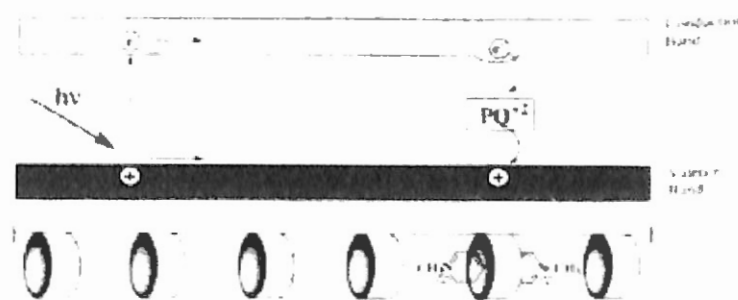
Figure 1: The Molecular Wire Approach

The experimental results of this study are presented in Figure 2 [7], where 3 and 2 are

monomers and the rest are AFPs. Static quenching dominates the quenching process for

the detectors in the upper pane; while dynamic quenching dominates in the lower pane.

The results of polymerization have increased the Stern-Volmer constant by a factor of

approximately 50 in the static case and approximately 15 in the dynamic case when

studied in solution. Increasing the Stern-Volmer constants directly translate to more

sensitive detectors.
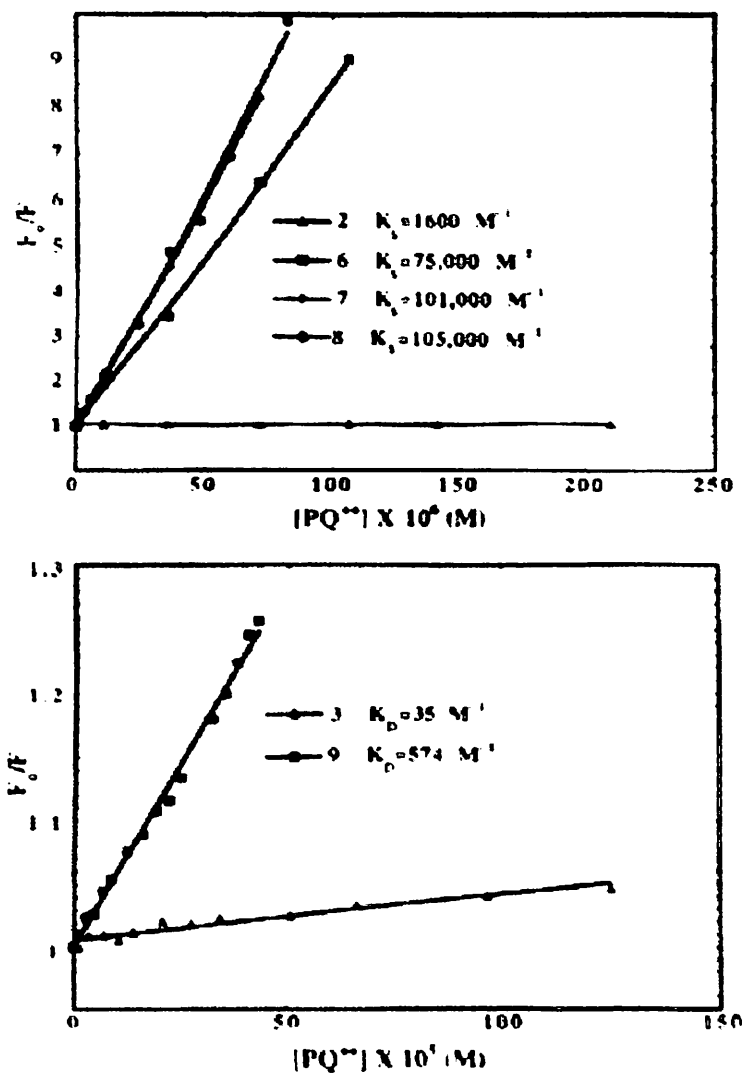
Figure 2: Stern-Volmer Constants for Monomers and Molecular Wire Polymers

A more explicit study of effect of the number of monomers repeated and the Stern-Volmer constants was done in the interest of developing biosensors [9]. They report two interesting findings. The first is a red shift and narrowing of both the absorption and the emission spectra as the length of the polymer grows. The second finding quantifies change in increase of the Stern-Volmer constant relative to a change in the number of repeat units in the polymer. The result for cyanine pendant poly(L-lysine) derivatives shows up to 250 polymer repeat units, the Stern-Volmer constant increases dramatically. However, increasing the number of repeat units beyond 250 led to only small increases in analyte sensitivity [9].

2.1.3 Related Polymers

This section discusses several polymers that operate on the same principle as the one used in this research, fluorescence quenching. These sensors tend to fall into two categories: biological sensors and chemical sensors with some of the more general work allowing for a sensor of both types. Also, although a selection of non-AFP sensors are discussed in this section, the majority are AFP based. The non-AFP sensors are explicitly noted.

Nomadics, Inc. has developed and tested a system for detecting nitroaromatics capable of vapor detection in the subfemtogram per kilogram range [8]. Detection is achieved by exciting an AFP-coated glass tube with the appropriate excitation wavelength and detecting the resulting fluorescence with a photomultiplier or avalanche photodiode. An interference filter is used to limit the light impinging on the detector to the appropriate

spectrum. This setup is shown in Figure 3. When ambient air is moved through the tube, if nitroaromatics are present, they quench the AFP, if nitroaromatics are not present, the clean air purges the analytes and the fluorescence recovers [10].
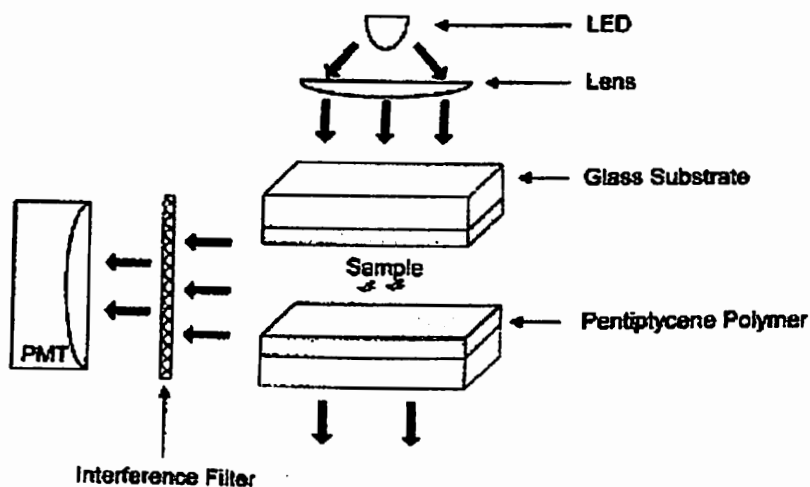
Figure 3: AFP Based Nitroaromatic Detector

One specific biologic application of non-AFP fluorescence quenching is the detection of chlorinated hydrocarbon containing pesticides, such as DDT, that do not break down in the environment [11]. By demonstrating that the fluorescence of carbazole-labeled phospholipids is dynamically quenched by the presence of several pesticides, including mirex, lidane, gardona, and DDE, the authors provide a method of detecting both the diffusion rates and the local concentration of these pesticides. Further, by demonstrating this effect with phospholipids vesicles containing 1 percent carbazole-labeling, [11] provides a potential tool for determining uptake and concentration of chlorinated hydrocarbon containing pesticides in cells.

A unique approach to using an AFP as a sensor was taken in [12]. The approach uses a quencher that will bind with the analyte that is being detected. If the result of the binding is a compound that no longer quenches the polymer, the fluorescence goes up. Specifically the work in [12] demonstrates the ability of N,N'-dimethyl-4,4'-bipyridinium (MV^{2+}) to quench [poly(2-methoxy-5-propyloxy sulfonate phenylene vinylene (MPS-PPV)] followed by a reduction in quenching (increase in fluorescence) with the addition of the protean avidin. This results from the weak binding of MV^{2+} and the MPS-PPV and a strong binding between the avidin and the MV^{2+}. The effect is that the avidin pulls the MV^{2+} away from the MPS-PPV and fluorescence is increased. The end result of this approach is that the fluorescence is off when avidin is not present and is on when the avidin is present [12]. Figure 4 demonstrates the fluorescence quenching and recovery. The solid line is the spectrum of MPS-PPV in water excited at 500nm. The bottom dash-dot line shows the spectrum of MPS-PPV in water after biotin-methyl viologen is added as a quencher. The middle dashed line is the spectrum of the quenched MPS-PPV after the addition of avidin. The top dotted line shows the spectrum with more avidin [12].
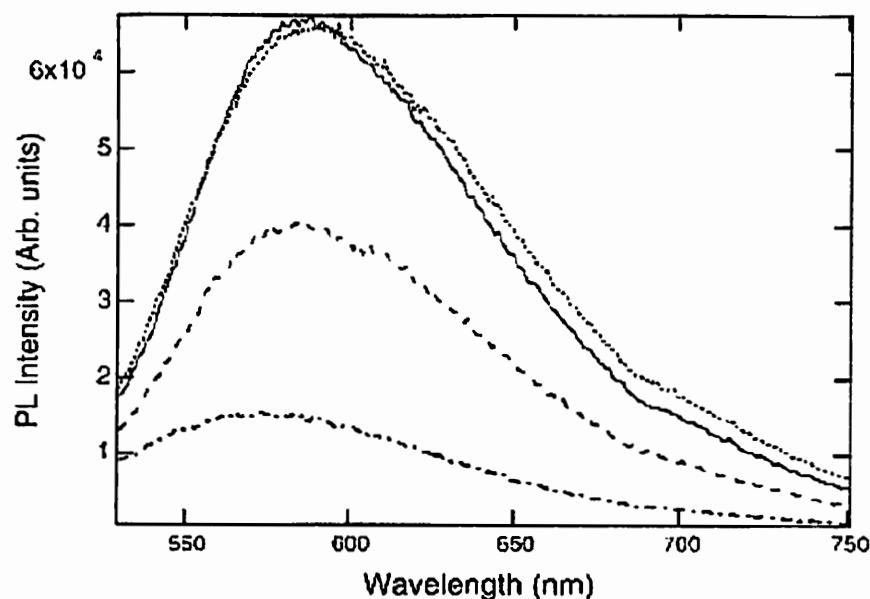
Figure 4: Quenching Recovery

Because there are many quenchers for MPS-PPV, this work may lead to sensors for several different proteins and biological macromolecules. To extend this work to chemical sensors, the authors demonstrate that a monolayer of MPS-PPV on a glass substrate performs similarly to MPS-PPV in an aqueous solution. By coating the MPS-PPV with other films sensitive and selective vapor-based sensors should be possible [12].

Additional work done at Nomadics, Inc. [13] demonstrates the use of an AFP in conjunction with stem-loop oligonucleotide (SLO) beacons for detecting possible biological warfare agents. Short chains of nucleotides, the building blocks of DNA and RNA, are referred to as oligonucleotides [14]. The stem-loop structure refers to a structure in which the compliment of the target is the loop and a short weakly binding section forms the stem. At one end of the structure is a fluorophore; while the other end has a quencher [15]. When the target sequence is not present, the weakly binding stem

12

holds the fluorophore and the quencher in close proximity. However, when the target is present, the loop binds to it forcing the more weakly bound stem apart, thus separating fluorophore and the quencher. As a result, when the target sequence is present, fluorescence is increased [13]. The stem loop structure is shown in Figure 5.
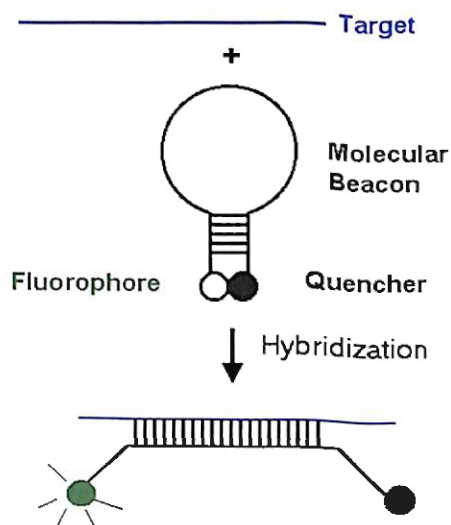
Figure 5: Stem Loop Oligonucleotide Sensor

Although the sensitivity of these stem-loop systems is less than the sensitivity of other detection schemes by several orders of magnitude, they have the advantage that they are capable of deployment in real time [13]. In order to increase the sensitivity [13] replaced the fluorophore with an AFP molecule designed for use in an aqueous environment and used fluorecein as a quencher. Positive identification of the target was demonstrated by an increase in emission at the wavelength of the AFP and a decrease in emission of the fluorecein when the system was excited by light at the excitation wavelength of the AFP [13].

The Stern-Volmer constants for the detectors discussed previously are on the order of $K_{SV} \approx 10^7 M^{-1}$. A significant jump in the Stern-Volmer constant, to a magnitude of $K_{SV} \approx 10^{11} M^{-1}$ was made by using gold nano-particles to quench polyfluorene [16]. By tethering the gold nano-particles to appropriate receptors, the techniques in [12] are applicable resulting in the potential for significantly more sensitive detectors. The authors of [16] claim that detection of analytes in the subpicomolar range should be achievable. Figure 6 shows the linear range, before the solution saturates, of the Stern-Volmer equation for this work. The data in this region demonstrates a Stern-Volmer constant of $K_{SV} \approx 5^{10} M^{-1}$.
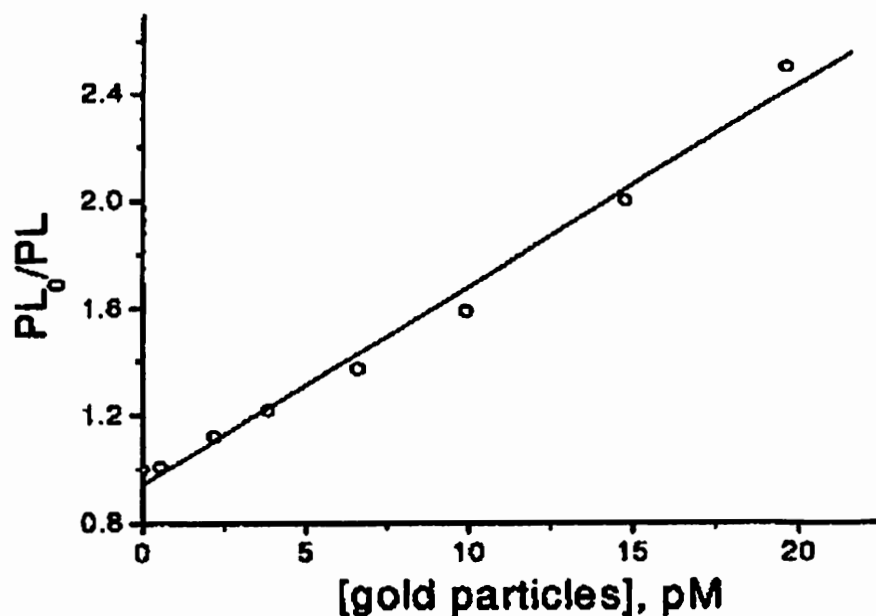
Figure 6: Stern-Volmer Plot of Polyflourene by Gold Nano-particles

2.2 CCDs

As stated above, this section discusses the current CCD and imaging technology available that could potentially be used for this application. A full review of the technology is neither feasible nor appropriate in this case because of the number of products available and the diversity of applications. Additionally, new CCDs are constantly being developed so it is important to consider the best current device at the time of development of the next generation of this system. The two major parts of this section are the desirable characteristics for the system and a discussion about a few of the CCDs currently available. A brief overview of the operation of CCDs precedes these sections and provides the necessary background for the following discussion.

2.2.1 Introduction to CCD Technology

Developed by Boyle and Smith in 1969 [17] the CCD has revolutionized imaging and has allowed for near real-time analysis in many applications. This section provides an overview of the desirable characteristics of an image sensor for this research before discussing the CCDs currently available. Additionally, the use of CCD mosaics, where several CCDs are used to form one large sensor, is briefly discussed.

2.2.2 Desirable CCD Characteristics

Like many other components, CCDs come in a wide range of styles and capabilities. The list below provides the ideal characteristics of a CCD for use in an application such as this research.

1. Large Number of Pixels
2. High Quantum Efficiency at the Emission Wavelength of the AFP and the Reference
3. Low Dark Current
4. Fast Readout
5. High Charge Transfer Efficiency (CTE)
6. Low Noise Readout Amplifier

The number of pixels determines the resolution of the system. A higher resolution results in capturing greater detail. The high quantum efficiency is required so that most of the photons that are incident on the surface of the CCD create electrons that can be detected on read out. This is particularly critical because of the small amount of light being collected by the system. A low dark current is important because thermally created electrons are indistinguishable from photogenerated electrons. In other words, a high dark current leads to an unacceptable level of noise. Given a CCD, there are two ways to control dark current. The first is to limit the amount of time of the exposure. If the system is capable of collecting a sufficient number of photons in a short time, the integration of the noise introduced by dark current is very low. Unfortunately, the system may not be capable of collecting sufficient light in a short period of time. A second method of controlling the dark current is to cool the CCD. A cooler CCD will produce significantly

fewer thermal electrons. In a related way, a fast readout helps by limiting the amount of time the electrons are stored in the CCD while no image is being captured. Also, fast readout allows for near real time analysis. The process of pushing electrons to the output amplifier can result in significant loss. The percent of electrons remaining after each move is the CTE. The number of electrons remaining after a series of moves is given by

$$n = n_0 \bullet CTE^r \tag{18}$$

where n is the number of electrons remaining after the moves, n_0 is the initial number of electrons, and r is the number of rows moved. A low CTE can be devastating. For example, moving 1000 electrons across 512 rows with a CTE of 99% results in only 6 electrons remaining at the end of the move. Any noise introduced by the readout amplifier propagates through the A/D and ends up in the final output. Therefore, even if the CCD itself is nearly ideal, a low-quality amplifier can cause poor results. Finally, the amplifier and the A/D need to have enough gain to allow for only a few photons per count which allows for a more precise measurement. The next section discusses several of the CCDs currently available and compares them according to the list above.

2.2.3 Analysis and Comparison of Currently Available CCDs

In this section, several CCDs, from several manufacturers, are compared and contrasted. The pros and cons of each are discussed and finally a summary is provided in the form of a table listing the critical parameters.

The CCD486 produced by Fairchild Imaging is 4096 pixels by 4097 pixels with an imager area of 61.44mm by 61.455mm [18]. This CCD is available in both front illuminated and back illuminated models. In the back illuminated version, the silicon has been thinned to approximately 18 microns and coated to increase sensitivity. At the wavelengths of interest, 460nm for the AFP and 590nm for the nano-particle core, the quantum efficiency of the CCD486 is approximately 90% when the UV enhanced AR coating is used [18]. In other words, nine out of ten incident photons create an electron. The CCD486 is expected to have a dark current of no more than 0.08 electrons per second when cooled to -60° C. The dark current approximately doubles for every 7° increase in temperature [18]. At the maximum readout frequency of 1 MHz, there is a maximum readout noise of 12 electrons per pixel. Finally, the gain of the output amplifier is nominally 3 uV/e- [18]. Fairchild Imaging used this CCD to develop the Peregrine 486 Camera, which incorporates a 16-bit analog to digital converter with 1.5 electrons per analog to digital unit [19].

The back-illuminated variation of the SITe S100A, the S100AB, is another CCD that might be suitable for this research. The size of the S100AB is only 2048 pixels by 2048 pixels and the quantum efficiency is only approximately 73% at 460nm and 80% at 590nm [20]. The readout rate is 10 MHz however, which is 10 times that of the CCD486. The dark current is no more than 30 pA/cm^2 at -15° C, which is an incredibly low 2.6 x 10^{-6} electrons per pixel per second. At 0° C this would be 1.2 x 10^{-5} electrons per pixel per second. Although the worst case CTE is 99.995%, which is the same as the CCD486, there will be fewer electrons lost because the S100AB is one quarter of the size of the

CCD486. Finally, the gain of the output amplifier is nominally 6 uV/e with a root mean square noise of no more than 6 electrons [20].

A third CCD, the CCD42-80, is designed for use as part of a mosaic or an array of CCDs. It is constructed such that several may be placed side by side with virtually no space between the edges of the sensing elements of each. Figure 7 is an image of the CCD42-80 [21]. If used as a single device, this CCD is 2048 pixels by 4096 pixels. By using a mosaic of six of these CCDs the number of pixels is increased to 4096 pixels by 6144 pixels. Additional CCDs would further increase the number of pixels available. The CCD42-80 has a quantum efficiency of about 88% at 460nm and about 85% at 590nm. The manufacturer claims dark current of 4 electrons per pixel per hour at -120° C. This converts to approximately 160.8 electrons per pixel per second at 0° C.
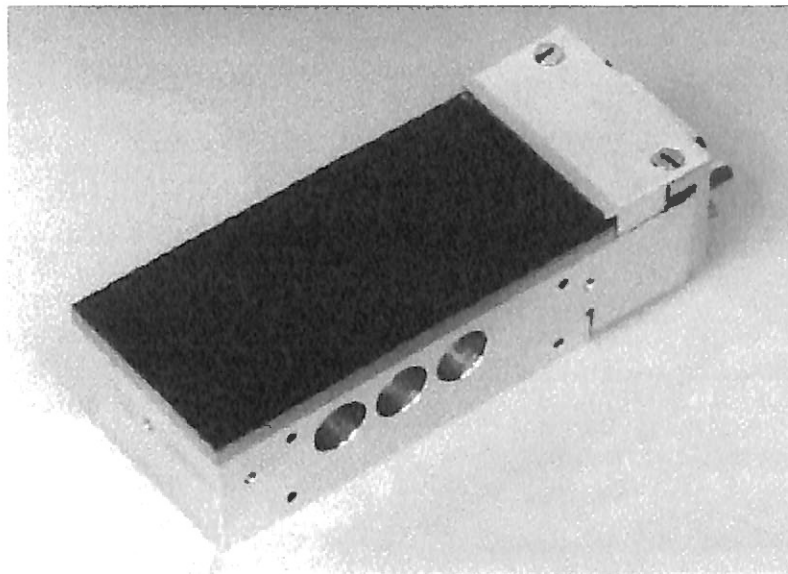
Figure 7: CCD42-80

The information presented above is summarized in Table 1. Because the nature of this research is proof of concept, and the CCDs discussed in this section can cost on the order of $100,000.00 [22], a smaller, less expensive CCD, the Kodak KAF0402ME, was used in this research. Its important parameters are listed in the Materials section of this thesis.

Table 1

Summary of CCD Characteristics

	CCD486 [18]	S100AB [20]	CCD42-80 [21]	CCD42-80 Mosaic (2x4)
Size (pixels)	4096 (H) x 4037 (V)	2048 (H) x 2048 (V)	2048 (H) x 4096 (V)	8192(H) x 8192 (V)
QE at 460nm (%)	91%	73%	88%	88%
QE at 590nm (%)	90%	80%	85%	85%
Maximum Dark Current at 0° C (electrons/pixel/second)	30.4	0.000012	160.8	160.8
Maximum Readout Frequency (kHz)	1000	10000	3000	3000 (each CCD read separately)
Minimum CTE (%)	99.995%	99.995%	99.999%	99.999%
Nominal Readout Amplifier Gain (V/electron)	3	6	4.5	4.5
Maximum Readout Noise (electrons/pixel)	12	6	4	4

3. EXPERIMENT

This section discusses the setup, execution, and result of the experimental procedure for this research.

3.1 Materials

The Santa Barbra Instrument Group (SBIG) ST-402 camera was chosen for this research because of its high quantum efficiency, low dark current, and reasonable cost. Figure 8 [23] shows quantum efficiency vs. wavelength for the KAF0402ME image sensor, which is the CCD installed in ST-402 camera. Figure 8 shows that the efficiency peaks in the visible range where this application requires the greatest sensitivity.

Figures 9 and 10 show the experimental set up. A high pressure Xenon lamp was used as a light source. The lab target was black felt with AFP coated nano-particle beads on it. Because of the near ideal background, no filter was needed to eliminate background noise. The field target was a dirt covered board with AFP coated nano-particle beads scattered on it. In the field, an extra filter was needed to eliminate the IR reflection of the arc lamp from the dirt.

A solution with concentration of 3.50 mg/ml of the analyte was sprayed on the target from approximately three inches away. The analyte sensitive 1mm diameter beads used in these measurements had cores doped with a nano-particle of poly-P-phenylene ethynylene-ZnS/Mn2+ composite material [24]. In principle, fluorescence of the core was to be used both to localize the bead and also as a reference intensity in conjunction with the measurement of the fluorescence intensity of the analyte sensitive coating to determine the presence or absence of the analyte. The coating of the beads was made of an AFP acting as a detector of analyte. The blue interference filter, Figure 10 [25], was a part of the original color wheel – a part of the ST-402 camera and is ideal for passing the spectrum of the AFP, shown in Figure 9 [26]. The florescence of the nano-particle doped core peaks at 590nm [27], so a 1mm-thick OG-590 filter placed in the color wheel of the camera was used to cut off wavelengths of less than 560nm. Finally, a BG-18 filter was placed on the objective lens of the camera. This filter blocked the infrared passed by the UG-11 filter on the illuminating arc lamp.

The following list summarizes the components of the system:

- Imaging System
    - Camera
        - SBIG ST-402 Astronomical Camera
        - Cooled Kodak KAF0402ME CCD
        - Low dark current
        - 16 bit analog to digital conversion
        - Sensitivity 1.5 electrons per count

- 765x510 pixels

- Internal computer controlled color filter wheel

- The green filter was replaced with the 1mm OG-590 filter used for the measurement of the reference signal

- The blue filter was used for measurement of the AFP signal

- BG-18 filter was placed on the objective lens of the camera in order to block IR

  o Lens

  - MTO1000A Maksutov telephoto lens, 1m focal length, f/10.5

- Light Source

  o Oriel 68806 Light Source, approximately 100W power

  o Xenon bulb

  o Operated at 6.3A

  o Output filtered by UG-11 filter

The software used, CCDOps, was developed by SBIG for use with their astronomical cameras. The software captured the image and provided a convenient way to change the contrast of the display. The software allowed the user to measure average intensity for a user-defined area surrounding a chosen pixel. The analysis of the results was done by hand according to the following process for several arbitrarily-selected beads in each set of images:

1. Find a bead or group of beads in the reference image made at 590 nm, and find the maximum intensity pixel in that image

2. Find the maximum intensity pixel for the same bead in the AFP image at 460 nm

3. Calculate the ratio of the maxima as well as the ratio of the average intensities of the surrounding area

Additional software processing could be done, however, to ensure consistency it is important to manually set the contrast parameters before exporting the images as bitmaps. A final product could potentially include digital-image processing software to identify and analyze the beads automatically. The current software provided with the camera is not very well suited for the task. For example, the process of exporting the images reduces the intensity scale from 16 bits to 8 bits.
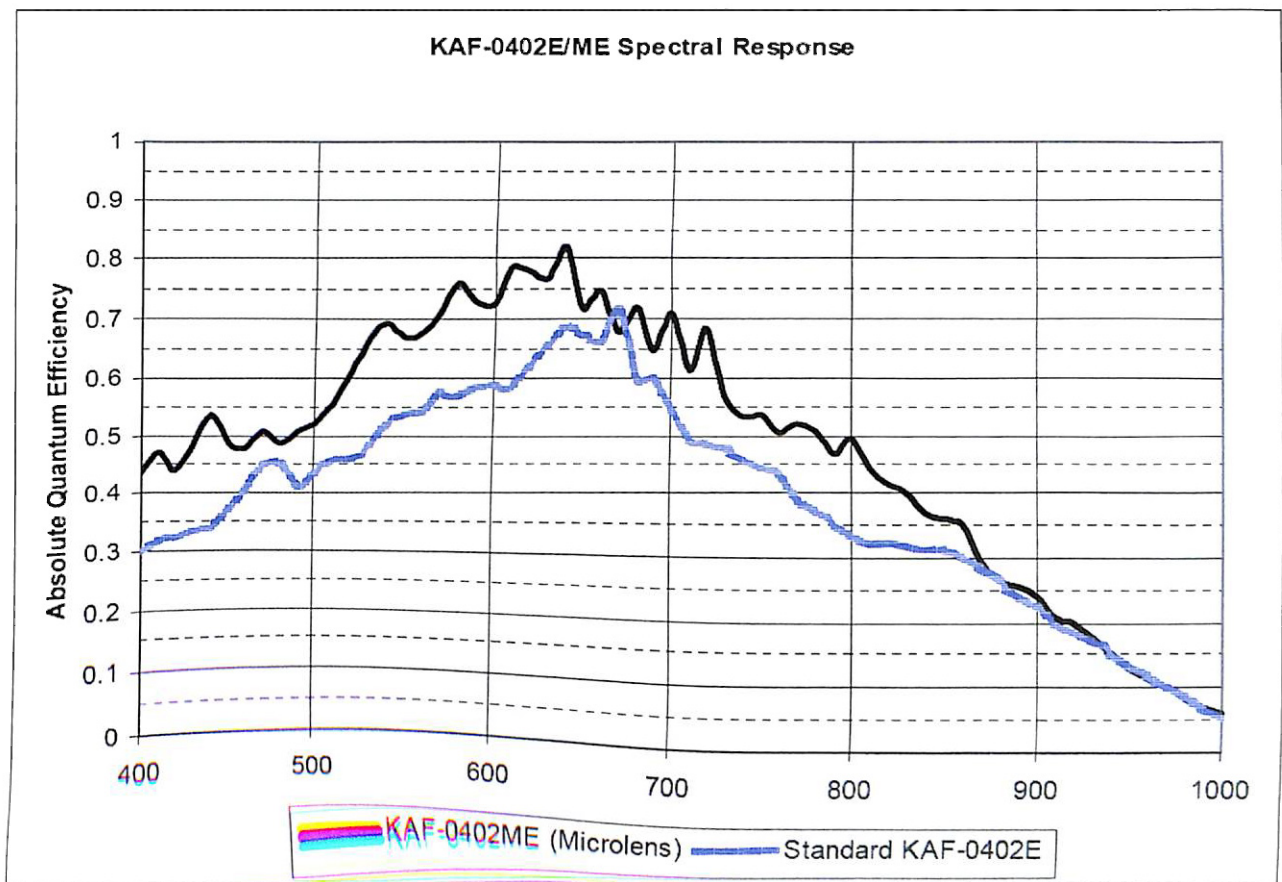
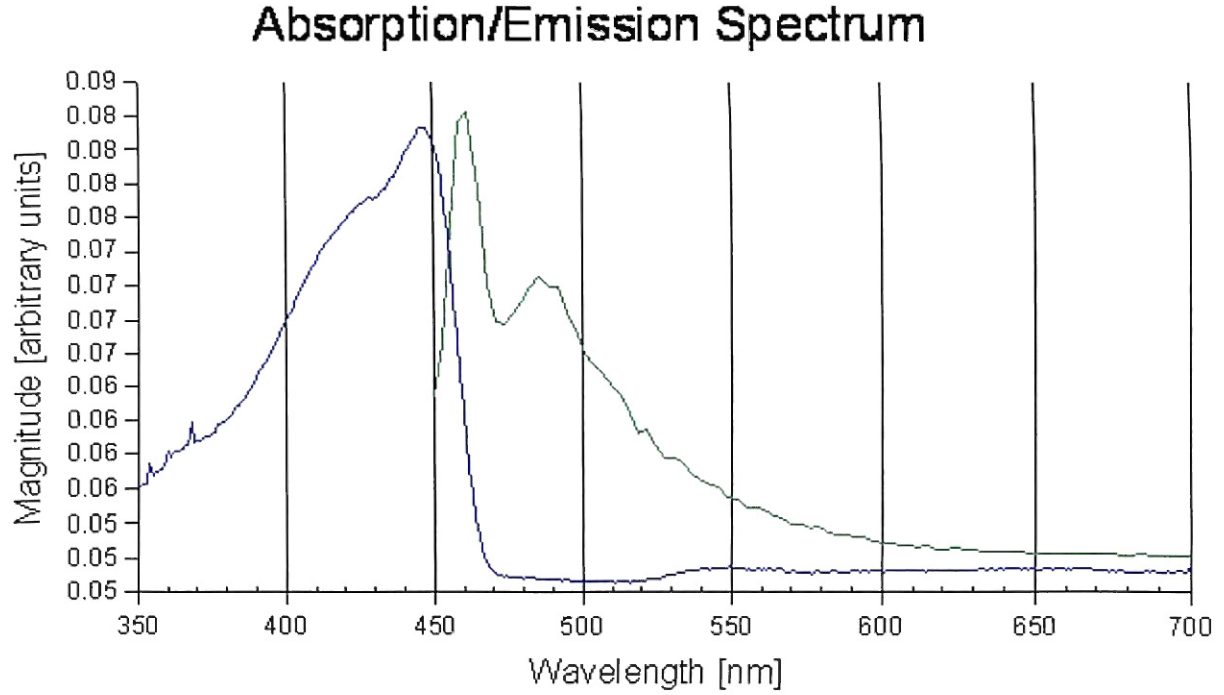**Figure 8: Sensitivity of the CCD vs. Wavelength [nm]**

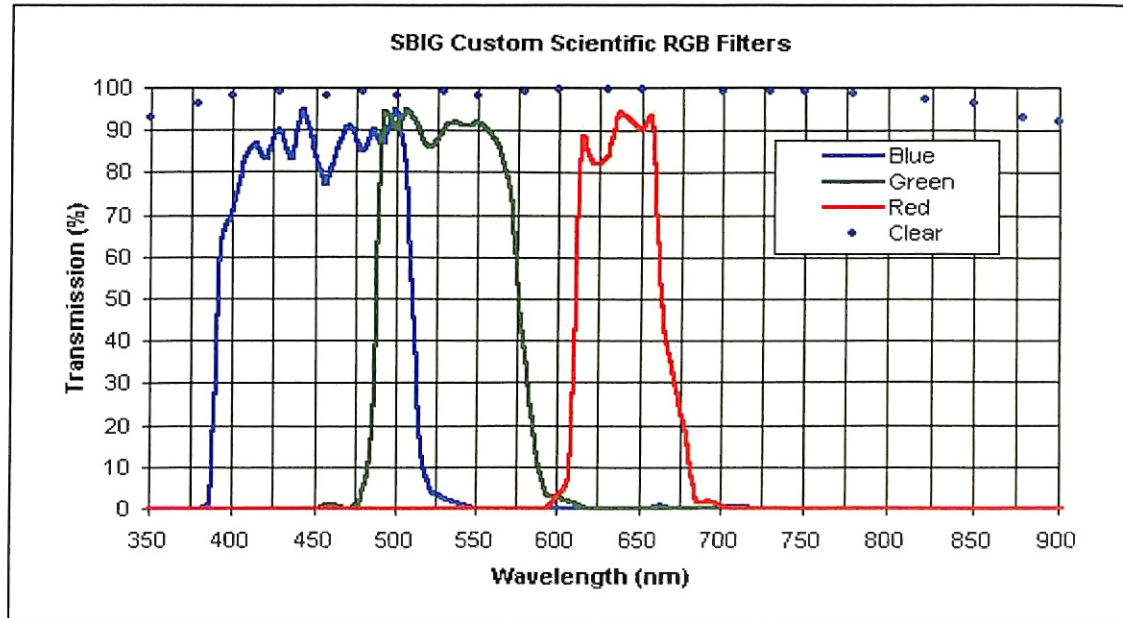**Figure 9:Absorption (blue) and Emission (green) Spectra of AFP**

Figure 10: Color Filters Supplied With the ST-402 Camera for Regular RGB

Pictures

3.2 Experimental Results

The investigative efforts were directed at proving the operation of the system at a distance between the camera and the beads equal to ~60 meters. Several lab tests were done to ensure that the system components would work together and that beads as well as the AFP signal could be detected using the camera with the filters. Additionally, images from the lab demonstrated the ability of the system to detect analyte. Unfortunately, the lab results were done without the BG-18 filter and the signal changes due to the presence of analyte were measured on a large background of IR passed through the UG-11 filter in the illuminator. Thus, relative changes of the AFP signal due to presence of analyte were rather small. The addition of an IR blocking BG18 filter in front of the camera was a key element in the final field test.

The field setup measured the presence of analyte at ~60 meters. These tests were purely binary (i.e. without analyte and with a large amount of analyte).

The detection capabilities of the camera are limited by noise of the measurements of the reference signal at 590 nm and detecting signal at 465 nm. The main source of noise is the shot noise due to limited number of photons.

Unfortunately, the series of beads used in the experiment exhibited very weak nano-particle core fluorescence at 590 nm, which was much weaker than the AFP fluorescence

signal at 465nm. As a result, our detection capabilities were limited by the calibrating signal from the nano-particle core.

The measured nano-particle core fluorescence was in the range of 750 electrons per exposure, which corresponds to the shot noise component of 27 and a relative noise/signal ratio of 3.65 %. The measured AFP fluorescence signals at 465nm were in the range of 1800 electrons, which produces signal to noise ratio of 2.36 %. The total signal to noise ratio in establishing concentration of analyte is equal to approximately 6.00 %

3.2.1 Summary of Lab Test Setup

The lab tests, using the setup shown in figure 4, were primarily to demonstrate the functionality of our camera and filter system rather than to demonstrate the ability of the AFP to detect the analyte. The lab setup and the field setup are identical with the following exceptions: the presence of the BG-18 filter in the field, the use of black felt as a backdrop in the lab vs. dirt in the field, difference in distance, and finally the use of a shorter and faster lens in the lab.
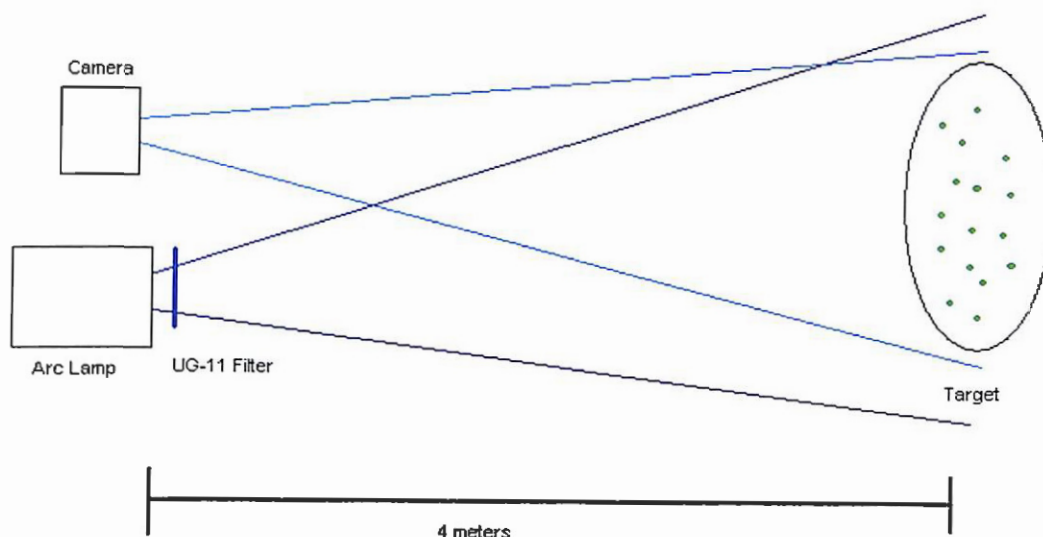
Figure 11: Setup of the System in the Lab

3.2.2 Summary of Field Test Setup

The field set-up is shown in figure 12. The target was a wooden board covered with dirt and sprinkled with detecting beads. The board was set at an angle of ~20 degrees off the horizontal plane. This way the camera had a view similar to a view seen by a camera mounted on a cherry picker or a helicopter. Reference images were taken before misting the beads and the dirt with analyte dissolved in toluene.
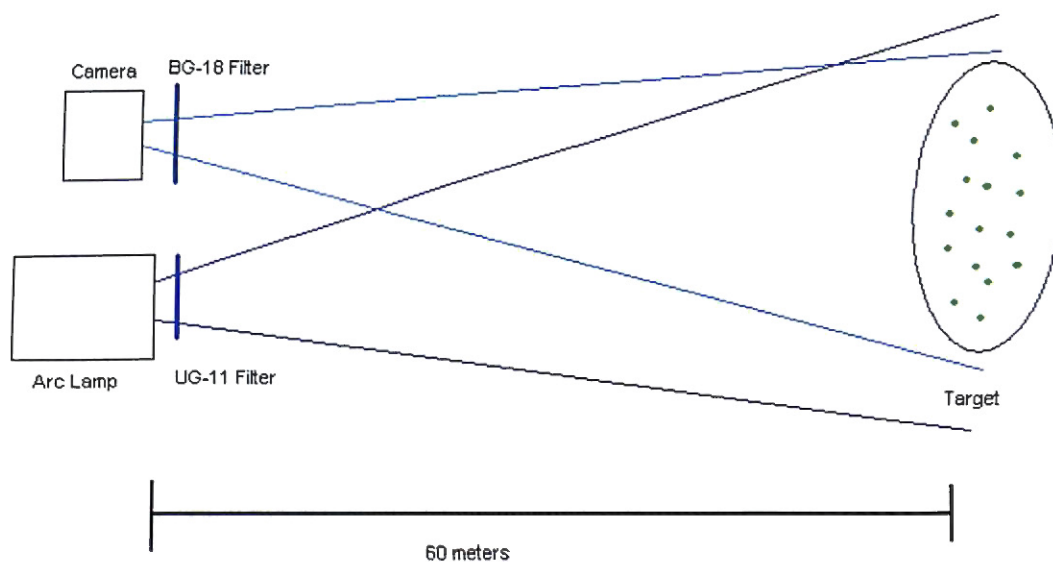
Figure 12: Setup of the System in the Field

3.2.3 Results of Lab Tests

The lab results proved promising enough for cause to continue on to a field test. The largest drawback of the lab results is that the BG-18 filter was not used meaning the CCD captured significant noise in the IR region. The four images below show two sets of beads, unexposed and exposed to analyte, with both the blue filter and the cutoff filter. Analysis of these images by averaging the intensities in a 3x3 window surrounding each maxima pixel for each bead yields a detector to reference ratio of 0.305 for the unexposed beads and 0.273 for the exposed beads.

Figure 13: AFP fluorescence (blue filter), 2 second exposure time, analyte exposed beads. Picture made from 4 meter distance using f/1.8 lens
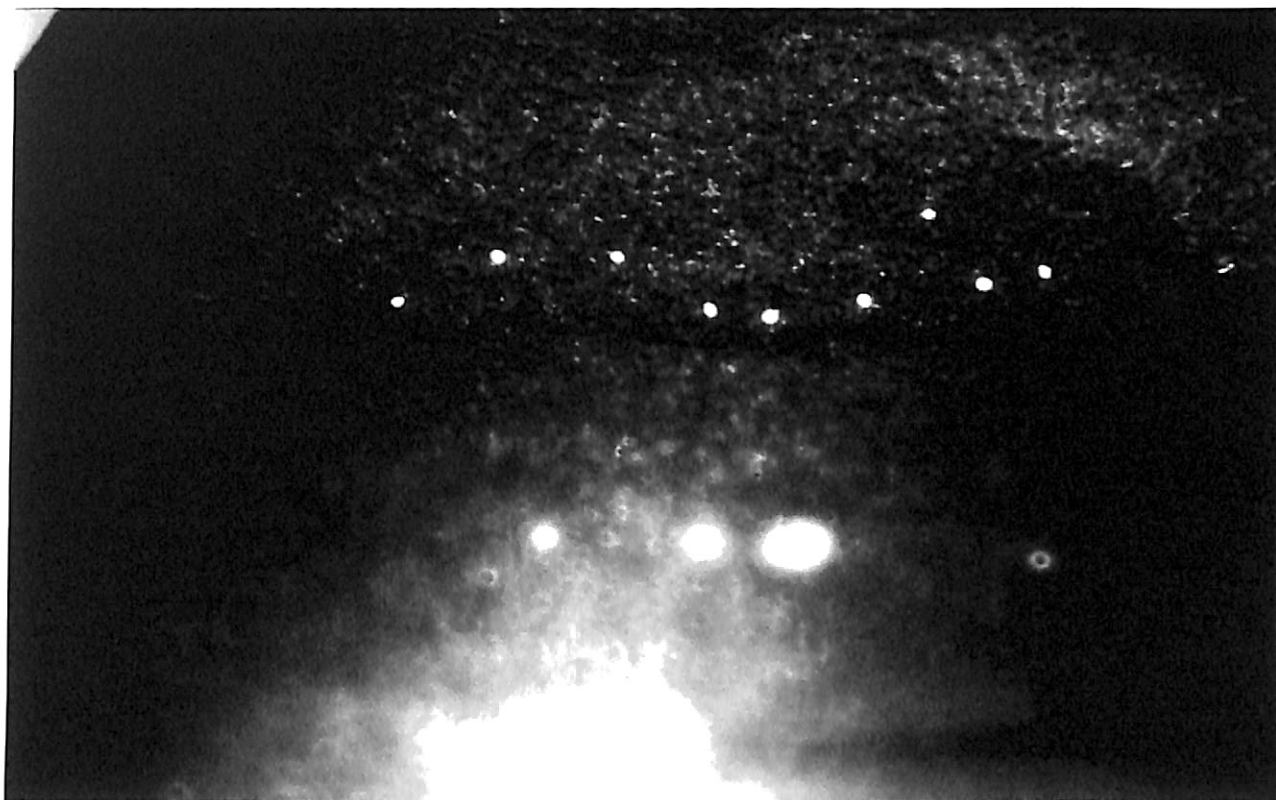
Figure 14: Nano-particle core fluorescence (OG-590), 0.04 second exposure time, analyte exposed beads. Picture made from 4 meter distance using f/1.8 lens

Figure 15: AFP fluorescence (blue filter), 2 second exposure time, beads not exposed to analyte. Picture made from 4 meter distance using f/1.8 lens

Figure 16: Nano-particle core fluorescence (OG-590 filter), 0.04 second exposure time, beads not exposed to analyte. Picture made from 4 meter distance using f/1.8 lens

3.2.4 Results of Field Tests

The tables below show the numerical analysis of the results.

x and y presented in Tables 2 and 3 show the position of the pixels corresponding to local maxima. Unfortunately, the board has shifted a little between measurements, so although the coordinates on different images vary, the beads were selected to be the same, i.e. the same bead or grouping of beads appears in each row of the table.

I5 - is the average intensity of a 5x5 pixel area surrounding the maxima.

Ip - is the intensity of the locally maxima pixel.

34

Ib - is the background intensity was determined by averaging three 31x31 pixel windows from areas of the image that appeared to be a reasonable representation of the background. It other words, the third and fourth column values are with respect to black, while the fifth and sixth column values are with respect to a grey background level. The intensities of the beads that have been exposed to analyte are denoted by analyte in the subscript.

Table 2

Blue Unexposed Maxima Intensities

x	y	I5	Ip	I5 - Ib	Ip - Ib
263	280	1690.0	1867	1248.5	1425.4
313	287	985.4	1097	543.8	655.4
263	224	750.2	807	308.6	365.4
269	316	601.9	670	160.4	228.4
245	289	944.4	1073	502.9	631.4
336	312	882.5	1010	440.9	568.4
313	325	792.0	872	350.5	430.4
424	264	813.6	1001	372.0	559.4

Table 3

Blue Exposed Maxima Intensities

x	y	I5analyte	Ipanalyte	I5analyte - Ibanalyte	Ipanalyte - Ibanalyte
261	308	882.0	972	427.1	517.0
313	321	838.2	929	383.2	474.0
269	252	636.9	682	181.9	227.0
265	341	512.2	602	57.2	147.0
243	317	709.1	792	254.1	337.0
333	349	937.5	1162	482.5	707.0
308	358	589.2	657	134.3	202.0
423	308	601.8	669	146.8	214.0

Table 4 provides additional analysis of Tables 2 and 3. Here the difference in intensity is clearly shown by dividing the locally maxima intensities of the exposed beads by the locally maxima intensities of the unexposed beads. In nearly every case, the ratio of the beads exposed to analyte with the beads not exposed to analyte is less than 0.9 when with respect to a black background and less than 0.75 when with respect to a representative grey level showing a significant quenching of the AFP fluorescence. Only in one case were the results not as expected. In this case we actually observed an increase in AFP fluorescence, which we are unable to explain.

Table 4

Exposed Maxima Intensities Divided By Unexposed Maxima Intensities

I5analyte / I5	Ipanalyte / Ip	(I5analyte – Ibanalyte) / (I5 – Ib)	(Ipanalyte – Ibanalyte) / (Ip – Ib)
0.522	0.521	0.342	0.363
0.851	0.847	0.705	0.723
0.849	0.845	0.589	0.621
0.851	0.899	0.357	0.644
0.751	0.738	0.505	0.534
1.062	1.150	1.094	1.244
0.744	0.753	0.383	0.469
0.740	0.668	0.395	0.383

Finally, Tables 5 and 6 present the intensity of AFP signal, I_{AFP}, in conjunction with the intensity of the reference signal from the nano-particle core, I_R. Due to the lower brightness of the reference, fewer groups of beads stood out from the background. However, there is still a clear difference in the signal to reference ratios. The average ratio, I_{AFP} / I_R, for the beads not exposed to analyte is 1.85 and the average ratio for beads exposed to analyte is 1.49, a percent difference of 21.6%. Even for the closest values, 1.64 for the beads not exposed to analyte and 1.60 for the beads exposed to analyte, the percent difference is 2.5%.

Table 5

Analysis of Unexposed Beads Including the Reference Signal

x	y	IR	IAFP	IAFP / IR
260	275	408.73	849.41	2.08
350	300	381.64	693.17	1.82
250	250	346.72	569.08	1.64

Table 6

Analysis of Exposed Beads Including the Reference Signal

x	y	IR	IAFP	IAFP / IR
260	300	441.08	635.69	1.44
275	275	356.36	507.27	1.42
350	330	358.64	573.56	1.60

The images below are the results of the field test. They are all displayed using the same contrast settings allowing for direct comparison, but reducing viewing quality.
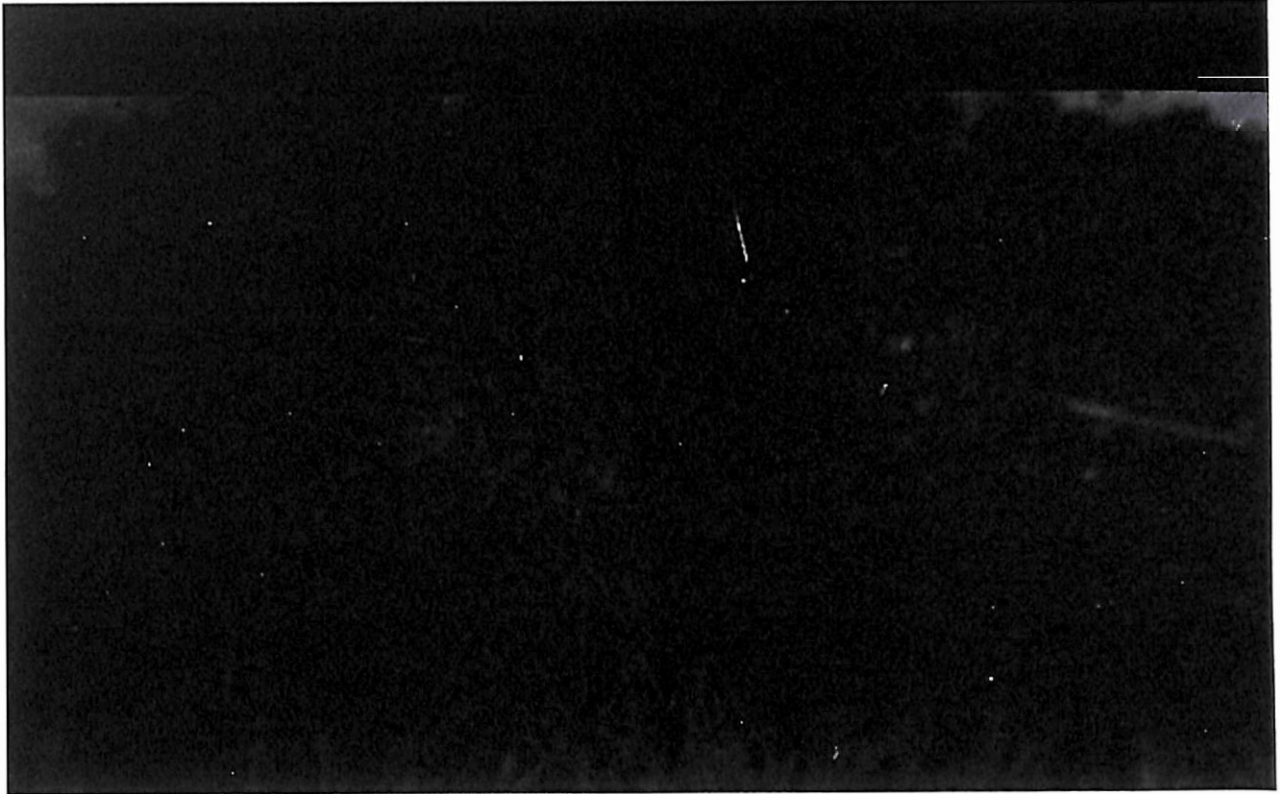
38

Figure 17: Nano-particle core fluorescence (OG-590 filter), 30 minute exposure time, picture made with an f/10.5 lens from a 60 meter distance, beads not exposed to analyte.

The beads are barely visible in Figure 17 because of the very small fluorescence intensity of the nano-particle core and the small dynamic range of this image. However the beads can be made very clear by using digital-image processing techniques which causes the common reference between images to be lost. Figure 18 shows the image after enhancement. Figure 19 shows the fluorescence of the AFP before being exposed to analyte.
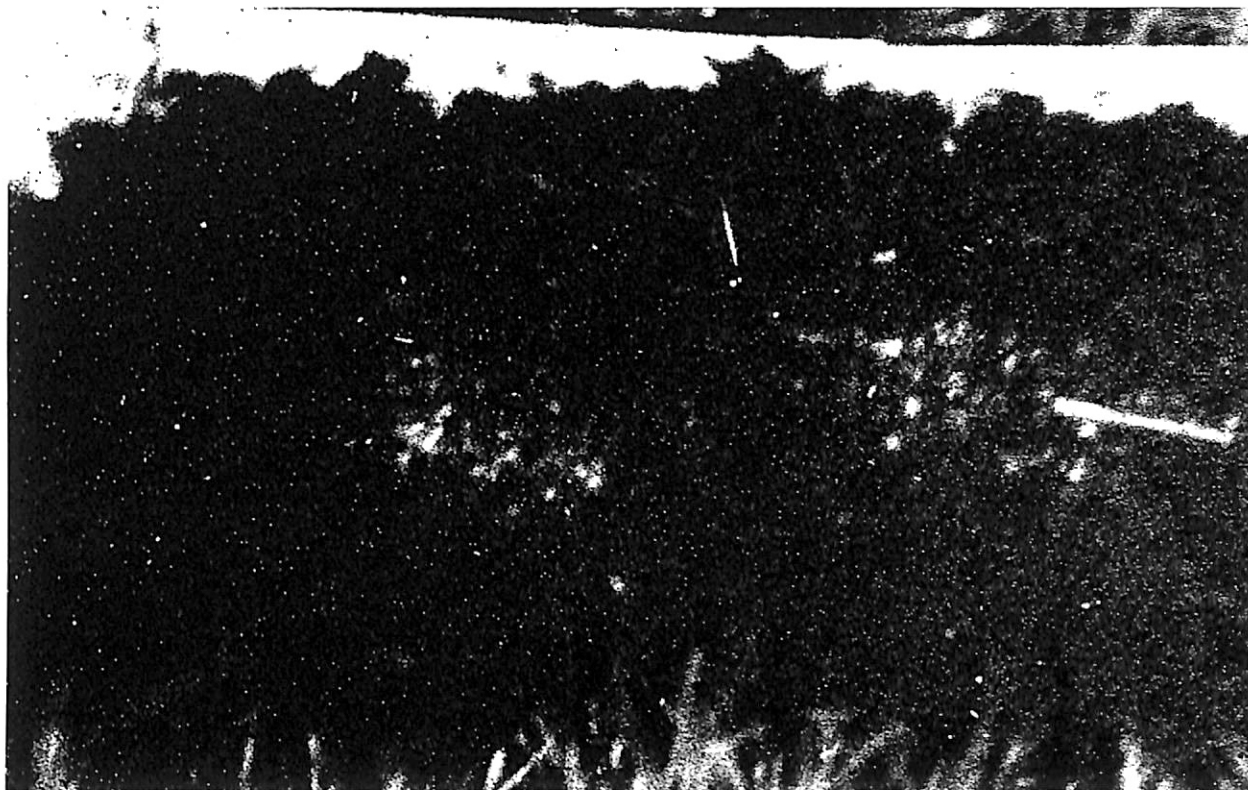
Figure 18: Nano-particle core fluorescence (OG-590 filter), 30 minute exposure time, picture made with an f/10.5 lens from a 60 meter distance, beads not exposed to analyte, contrast and black level adjusted

Figure 19: AFP fluorescence (Blue filter), 30 minute exposure, picture made with an

f/10.5 lens from a 60 meter distance, beads not exposed to analyte

Figure 20: Nano-particle core fluorescence (OG-590 filter), 30 minute exposure time, f/10.5 lens, 60 meter distance, beads exposed to analyte.

The beads are invisible in Figure 20 because of the very small fluorescence intensity of the nano-particle core and the small dynamic range of this image. Figure 21 shows the same image after contrast and black level adjustment. Figure 22 shows the fluorescence of the AFP after exposure to the analyte.
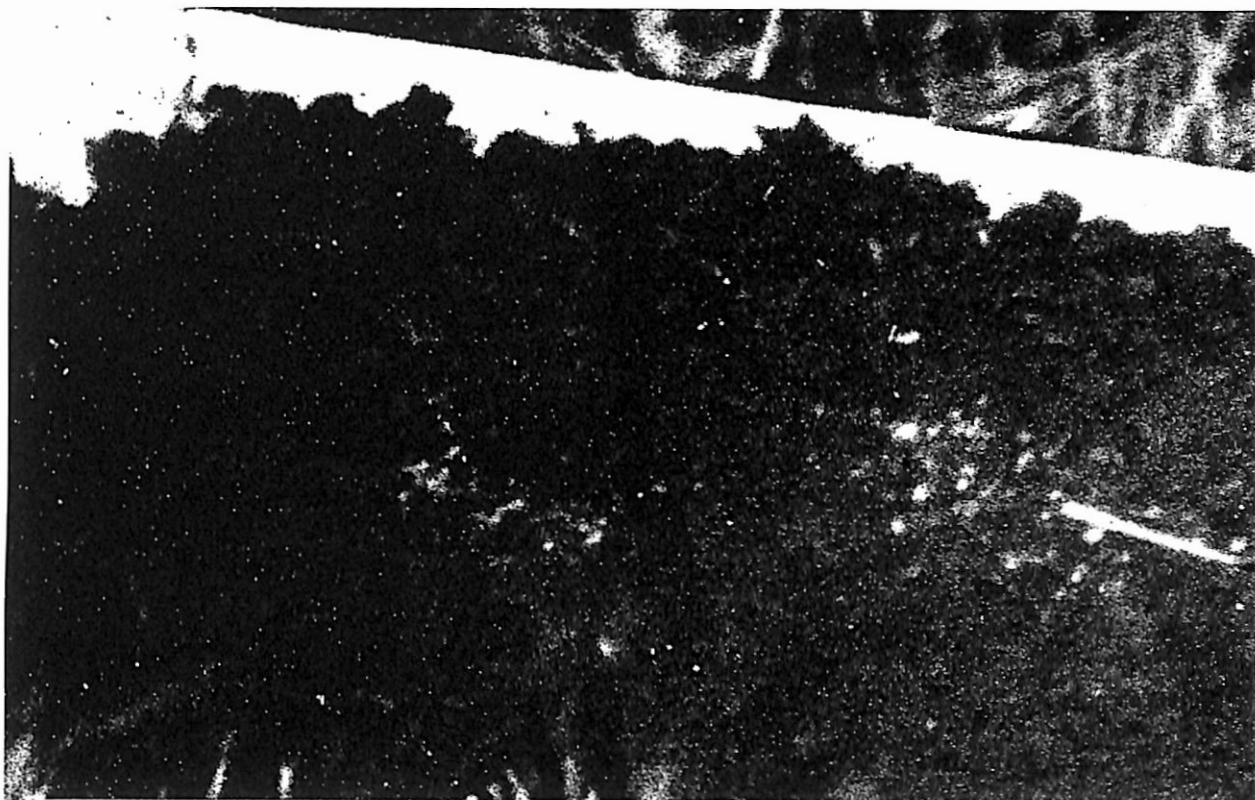
Figure 21: Nano-particle core fluorescence (OG-590 filter), 30 minute exposure time, f/10.5 lens, 60 meter distance, beads exposed to analyte, contrast and black level adjusted
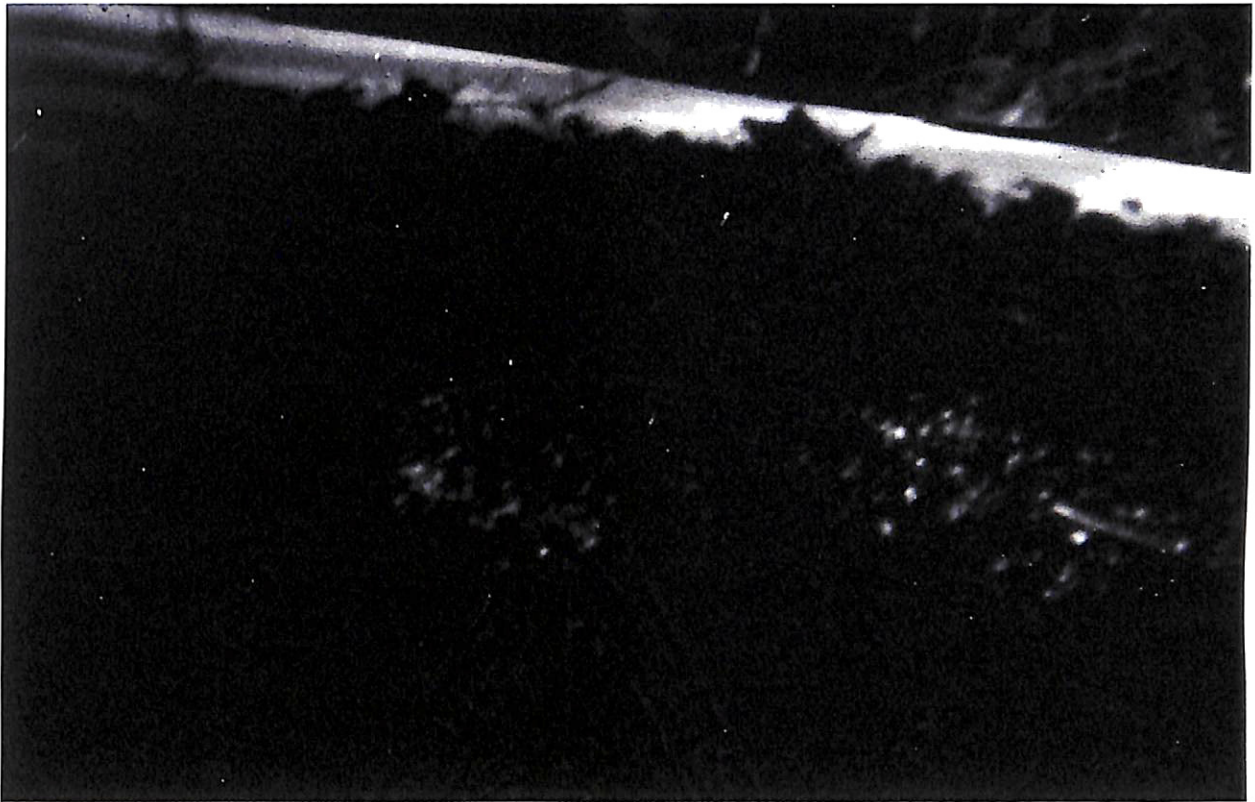
Figure 22: AFP fluorescence (Blue filter), 30 minute exposure, picture made with an f/10.5 lens from a 60 meter distance, beads exposed to analyte

3.3 Recommendations for further investigations

Unfortunately, the ability to detect the beads was not limited by the thin layer and small amount of ATP, but by the weak 590nm fluorescence of the core. That significantly reduced ability to identify the beads in images. Also, this fluorescence signal was used for calibration of the AFP signal, and that increased the noise of the normalized ATP signal. In fact the signal at 590 was so weak that we used the 465 AFP signal to identify the beads in the images, and the exposure time for the 590nm was unnecessarily long. Design of these beads should be revised. It seems that it would be very simple to use easily accessible and inexpensive, strongly fluorescing dye like Rhodamine 6G, or

44

similar, instead of the exotic nano-particles, for calibrating purposes. These dyes are environmentally friendly, and they would produce much higher signal at approximately the same wavelength as currently used nano-particles.

The beads used in the experiment were approximately 1mm in size and this size at a distance of 60m is close to the resolution limit of the lens. The small size coupled with weak signal made single beads difficult to find in the image. It seems that larger beads, approximately 3 - 5 mm in diameter, or perhaps even bigger, would significantly help in measurements. Covering several pixels, beads like that would be much easier to localize in the pictures. Additionally one could operate with a shorter exposure time using the average of the signal from the several pixels covering the bead. A 5mm bead would provide a total signal increase, when integrated over the surface, proportional to the increase of the projection surface of the bead (i.e. equal to 25x). A larger bead would also allow application of lens with shorter focal length (i.e. with larger field of view for a constant size of CCD array).

Exposure time in this research was rather long due to the non-optimal imaging lens and the weak illumination system, and the already discussed weak fluorescence of the nano-particle core; however the camera was rather good. The lens used in the experiment was a common inexpensive telephoto lens with f/10.5. Reducing this to f/2.8 would result in approximately a 16x reduction of exposure time.

Exchanging the general purpose filters used in this setup for customs-built interference filters with a higher transmission at the wavelengths of the reference and the AFP fluorescence, and more attenuation away from these wavelengths would improve the system's performance. Additionally, filters with some IR transmission, shown in the Figure 21, were used in this research. The peak of the residual transmission was approximately equal to 2.5×10^{-3}. Further reduction of IR transmission would be beneficial. However, one can not expect a dramatic improvement due to such changes. Perhaps a factor of 2x in shortening of exposure time would be possible.
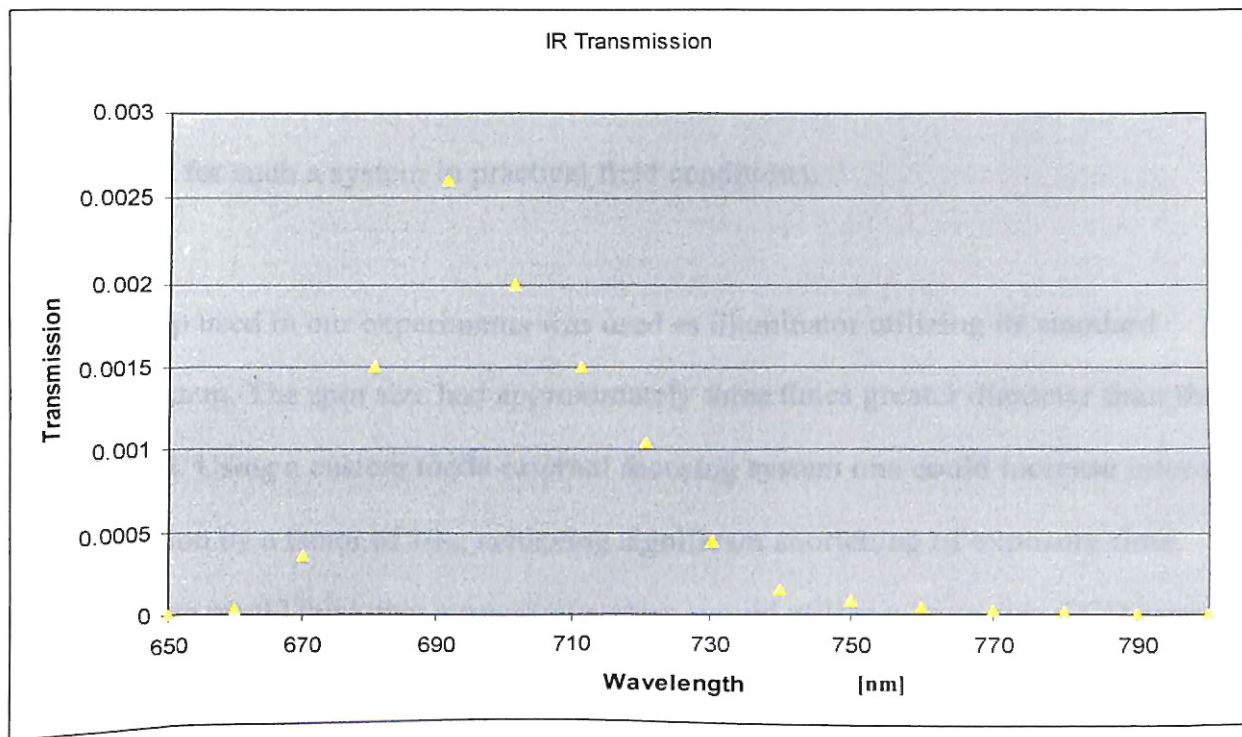

Figure 23: Residual IR transmission through 2 mm of UG11 together with 1mm of BG18

The CCD camera used in these measurements had a very good sensitivity. However, it was a very small cheap device produced for amateur astronomers. Its small number of pixels, slightly over 0.39 Mpixels, and small size, of 31.8 mm^2, could cover rather a small

area with a limited resolution. For a camera used in a practical system, a large size CCD is a must. CCDs like that are on the market. For example, Fairchild currently has available a 16 Megapixel CCD that is slightly over 60x60 mm square in size [18]. There are also CCDs with arrays covering the whole front surface without margins, produced for astronomical and other applications. Such detectors can be installed one next to another producing a mosaic with a very high resolution.

We used a rather low power (i.e. 100W) high pressure arc lamp for illumination purposes. Increasing the lamp power to approximately 1KW would result in 10x reduction of exposure time. Even higher power arc lamps are available, which would produce even shorter exposure times; however, it is not certain how much power would be available for such a system in practical field conditions.

The arc lamp used in our experiments was used as illuminator utilizing its standard focusing system. The spot size had approximately three times greater diameter than the imaged field. Using a custom made external focusing system one could increase intensity of illumination by a factor of 10x, achieving significant shortening of exposure time. However, one would think that a practical system would utilize a large size CCD array; therefore, it is doubtful if the factor of 10x would be achievable. Nevertheless, one should carefully design the illuminating system in order to deliver most of the available light output to the imaged area.

Using only a few of discussed improvements (i.e. larger beads, better lens, better filters and stronger 1KW light source) would reduce exposure time by a factor of 25x16x2x5=4000 and further improvement of the system by design of better optics for the illuminating beam is still possible. Even this 4000 factor alone reduces the exposure time of 30 minutes used in our experiments to less than a half of a second, making the system much easier to use and providing images in near real-time. Also, if an active stabilization of the camera was used, it would make it possible to acquire images from a moving car or a helicopter.

4. CONCLUSION

The result of this research is a system that is capable of detecting specific trace analytes at a distance of 60 meters. The equipment used was standard off-the-shelf components modified to fit the specific needs of this project. A background of the AFP has shown its superiority to a single chromophore sensor for this application. Additionally, desirable CCD characteristics have been discussed and three CCDs have been compared in terms of those characteristics. Finally, the experiment is presented in three parts: The materials, the experimental results, and recommendations to improve the system.

BIBLIOGRAPHY

[1]   National Research Council (U.S.). Committee on the Review of Existing and Potential Standoff Explosives Detection Techniques, *Existing and potential standoff explosives detection techniques / Committee on the Review of Existing and Potential Standoff Explosives Detection Techniques, Board on Chemical Sciences and Technology, Division on Earth and Life Studies, National Research Council of the National Academies.* Washington, D.C.: National Academies Press, 2004.

[2]   D. L. Woolard, E. R. Brown, A. C. Samuels, J. O. Jensen, T. Globus, B. Gelmont, and M. Wolski, "Terahertz-frequency remote-sensing of biological warfare agents," presented at Microwave Symposium Digest, 2003 IEEE MTT-S International, 2003.

[3]   D. T. McQuade, A. E. Pullen, and T. M. Swagger, "Conjugated Polymer-Based Chemical Sensors," *Chemical Reviews,* vol. 100, pp. 2537-2574, 2000.

[4]   A. W. Czarnik, "Supramolecular Chemistry, Fluorescence, and Sensing," in *Fluorescent Chemosensors for Ion and Molecule Recognition,* A. W. Czarnik, Ed. Washington, D.C.: American Chemical Society, 1993, pp. 1-9.

[5]   N. N. Barashkov and O. A. Gunder, *Fluorescent Polymers.* London: Ellis Horwood, 1994.

[6]   J. R. Lakowicz, *Principles of Fluorescence Spectroscopy.* New York, New York: Plenum Press, 1983.

[7]   Q. Zhou and T. M. Swager, "Methodolgy for Enhancing the Sensitinity of Fluorescent Chmosensors: Energy Migration in Conjugated Polymers," *Journal of the American Chemical Society,* vol. 117, pp. 7017-7018, 1995.

[8]   L. F. Hancock, R. Deans, J. Moon, and T. M. Swager, "Amplifying Fluorescent Polymer Detection of Bioanalytes," 2002.

[9]   R. M. Jones, L. Lu, R. Helgeson, T. S. Bergstedt, D. W. McBranch, and D. G. Whitten, "Building Highly Sensitive Dye Assemblies for Biosensing from Molecular Building Blocks," *Proceedings of the National Academy of Sciences of the United States of America,* vol. 98, pp. 14769-14772, 2001.

[10]   C. J. Cumming, C. Aker, M. Fisher, M. Fox, M. J. l. Grone, D. Reust, M. G. Rockley, T. M. Swager, E. Towers, and V. Williams, "Using Novel Fluorescent Polymers as Sesory Materials for Above-Ground Sensing of Chemical Signature Compounds Emanating from Buried Landmines," *IEEE Transactions on Geoscienc and remote sensing,* vol. 39, pp. 1119-1128, 2001.

[11]   G. Omann and J. R. Lakowicz, "Pesticide Uptake into Membranes Measured by Fluorescence Quenching," *Science,* vol. 197, pp. 465-467, 1977.

[12] L. Chen, D. W. McBranch, H.-L. Wang, R. Helgeson, F. Wudl, and D. Whitten, "Highly sensitive biological and chemical sensorsbased on reversible fluorescence quenching in a conjugated polymer," *Proceedings of the National Academy of Sciences of the United States of America*, vol. 90, pp. 12287-12292, 1999.

[13] B. D. Clinkenbeard, A. Ramachandran, J. R. Malayer, J. H. Moon, and L. F. Hancock, "Stem-loop oligonucleotide beacons as switches for amplifying fluorescent polymer based biological warfare sensors," *Proceedings of SPIE*, vol. 5071, pp. 272-279, 2003.

[14] W. S. Klug, M. R. Cummings, and C. A. Spencer, "Concepts of Genetics," eighth ed. Upper Saddle River, New Jersey: Pearson Education, Inc., 2006, pp. 243.

[15] S. Tyagi and F. R. Kramer, "Molecular Beacons: Probes that Fluoresce upon Hybridization," *Nature Biotechnology*, vol. 14, pp. 303-308, 1996.

[16] C. Fan, S. Wang, J. W. Hong, G. C. Bazan, K. W. Plaxco, and A. J. Heeger, "Beyond Superquenching: Hyper-Efficient Energy Transfer from Conjugated Polymers to Gold Nanoparticles," *Proceedings of the National Academy of Sciences of the United States of America*, vol. 100, pp. 6287-6301, 2003.

[17] W. S. Boyle and G. E. Smith, "Charge Coupled Semiconductor Devices," *Bell System Technical Journal*, vol. 49, pp. 587-593, 1970.

[18] Fairchild Imaging, "CCD486 4k x 4k Image Area Full Frame CCD Image Sensor," 2004.

[19] Fairchild Imaging, "Perigrine 486."

[20] SITe, "SITe S100A 2k x 2k 12um Charge-Coupled Device Family." Tigard, OR, 2003.

[21] e2v Technologies, "CCD42-80 Back Illuminated High Performance CCD Sensor." Elmsford, NY, 2003.

[22] Fairchild Imaging, (Private Communication), 2006

[23] Kodak, "Device Performance Specifications KAF-0402E/ME," in *768 (H) x 512 (V) Enhanced Responce Full-Frame CCD*, 2003, pp. 17.

[24] W. Chen, A. P. Woly, T.-O. Malm, T.-o. Bovin, and S. Wang, "Full-Color Emission and Temperature Dependence of the Luminescence in Poly-P-phenylene ethynylene-ZnS/Mn^{2+} Composite Particles," *The Journal of Physical Chemistry B*, vol. 107, pp. 6544-6551, 2003.

[25] Santa Barbra Instrument Group, "Online Catalog Page," vol. 2005, 2006.

[26] T. Douglas, (Private Communication), 2005

[27] C. Wichert, (Private Communication), 2005

VITA

Robert James Sleezer

Candidate for the Degree of

Master of Science

Thesis: STANDOFF TRACE ANALYTE DETECTION USING AMMPLIFYING

FLUORESCENT POLYMERS

Major Field: Electrical Engineering

Biographical:

Education: Graduated from Stillwater High School, Stillwater, Oklahoma in May 1997; received Bachelor of Science degree in Computer Science and a Bachelor of Science degree in Electrical Engineering. Completed the requirements of the Master of Science degree with a major in Electrical Engineering at Oklahoma State University in May 2006.

Experience: Employed as summer camp staff at Will Rogers Scout Reservation and Lost Lake Scout Reservation Summers; employed by Oklahoma Lions Boys Ranch as relief ranch parent; employed by Oklahoma State University as an undergraduate and graduate research assistant and as an undergraduate and graduate teaching assistant; Oklahoma State University, Department of Electrical Engineering, 2001 to present

Professional Memberships: The Institute of Electrical and Electronics Engineers, SPIE the International Society for Optical Engineering